

CHAPTER 5: Description of the Experimental Setup

Until now the theoretical grounds of homogeneous ice nucleation in supercooled liquid water was considered. In this context, we challenged to relate the structural properties of liquid water to the dynamics of homogenous ice nucleation. We presented our points of view in terms of a modified statistical thermodynamic model of liquid water, and developed a new kinetic approach to the formation of critical ice-germ.

In this chapter, we present the description of our experimental setup: The experiments are conducted by levitating single droplets of 40- 70 microns sized in an electrodynamic balance. The droplet properties are analyzed by Mie light scattering.

Levitated single droplet experiments do comparatively stay as a new kind of measurement technique to study the nucleation behaviour in the liquid phase. Working with single droplets offers high purity and no surface contact for the samples. Furthermore it allows obtaining more accurate results on the statistics of nucleation times in comparison to emulsions or expansion-cloud chambers.

5.1 Previous Measurements

The measurement of homogenous nucleation rates in liquid phase could be achieved with different experimental techniques. These techniques may vary from each other in the sampling process, or in the detection of the nucleation events. A list of experimental methods and equipment that are suitable to measure the nucleation rates is given by Koop (Koop 2004). These methods are capillary and emulsion techniques (Angell 1983), cloud expansion chambers (Hagen, Anderson et al. 1981; Demott and Rogers 1990; Möhler, Stetzer et al. 2003), continuous flow diffusion chambers (Chen, Demott et al. 2000), FTIR flow tubes (Bertram, Patterson et al. 1996), droplet drain tubes (Wood, Baker et al. 2002), optical microscopy (Koop, Molina et al. 1998; Salcedo, Molina et al. 2000) and levitated droplet experiments (Kramer, Hübner et al. 1999; Stöckel, Weidinger et al. 2004; Stöckel, Weidinger et al. 2005). Among these techniques the emulsion and cloud expansion chambers are long-established methods that commonly apply to the measurement of the nucleation rates.

In the emulsion technique the sample is emulsified as small droplets in a dispersant phase. The droplets are isolated by covering their surfaces with an inert surfactant. As an example the dispersant phase could be a 1:1 volume mixture of methylcyclopentane and methylcyclohexane, and the surfactant could be sorbitan tristearate (Span 65) (Miyata and Kanno 2005). The emulsion is prepared using a blender at a certain rotating rate. In the measurement stage, emulsified droplets are first cooled down. The cooling rate is usually on the order of 10 degrees per second. The nucleation event is detected by differential scanning calorimetry (DSC).

This technique as it is described here was formerly developed by Rasmussen and MacKenzie and widely applied to investigate the behavior of supercooled liquid water (Rasmussen and MacKenzie 1973). In addition Angell et al (Angell 1983) studied the nucleation behavior of supercooled liquid water and aqueous solutions with emulsified samples.

One disadvantage of the emulsion experiments is that, it is not possible to obtain single droplet statistics. The homogeneous nucleation temperature (T_H) is determined as a point, where certain amount of (90 %) droplets is frozen. Another disadvantage is the use of surfactants to emulsify the samples. Possible influence of the surfactants to the homogenous nucleation behaviour is

recently discussed by Tabazadeh et al (2002)(Tabazadeh, Djikaev et al. 2002), considering the surface crystallization of supercooled liquid water.

The cloud expansion chamber experiments are used primarily to study the vapor to liquid condensation(Volmer and Flood 1934; Allard and Kassner 1965; Wölk and Strey 2001); however can also be applied to freezing experiments(Hagen, Anderson et al. 1981). In the condensation experiments a gaseous sample at high vapour pressure is expanded into a chamber in which the sample is being probed and its temperature is adjusted. During the expansion, the temperature of the gas falls down and it becomes supersaturated. Further supersaturations can be achieved by applying pressure pulses to the chamber from an inlet valve (Wölk and Strey 2001). Homogenous nucleation of the sample is also achieved by means of a nucleation pulse. The formation of the liquid droplets is detected by analyzing the Mie scattering of light from the sample.

Similar to emulsion experiments the cloud expansion chamber experiments does not allow analyzing single droplet statistics. They also suffer from the wide size distribution of the particles, which results in lower precision in determining the homogenous nucleation rates.

Levitated droplet experiments are becoming more popular not only to study the nucleation rates but also to study the various thermodynamic kinetic and optical properties of aerosol particles(Hamza 2004). These kinds of experiments are based on trapping a single droplet (or a solid particle) into a small region of stability. This can be achieved by optical (Rühl –Raday Discuss.), acoustic or electrodynamic (Kramer, Hübner et al. 1999) levitation. In advance, the size, composition, index of refraction and the physical state of the particle can be analyzed by getting use of elastic light scattering phenomena.

In studying the homogeneous ice nucleation; an important task is to purify the sample from any kind of impurities, which may induce heterogeneous nucleation. . If there exists any nucleating agent in the whole sample, dividing it into small pieces would localize the heterogeneous nucleation only to few samples of small size, ensuring the others will nucleate homogeneously(Koop 2004). Besides, how pure the sample is prepared; the question of “How safe is the contact of the sample to the container surface?” should be considered to prevent

heterogeneous nucleation. For this reason, the levitated droplet experiments seem promising, which reduces the risk of heterogeneous nucleation, by handling the sample without any surface contact, and by allowing, probing of very-small-sized droplets one at a time.

In the research group of Professor Helmut Baumgärtel, in Freie University – Berlin two electrodynamic traps were constructed to investigate the freezing processes of supersaturated solutions. Previously, experiments were performed to study the homogeneous nucleation behavior of supercooled liquid H₂O and D₂O(Stöckel 2001), electrolyte solutions(Klein 2002), and n-alkanes with long chains(Weidinger 2003). Current research extends the measurements to homogeneous nucleation of ice in supercooled liquid mixtures of water with non-electrolytes. We investigate the homogenous nucleation behavior of supercooled liquid mixtures of water with ethanol, isopropanol, glycol, 1, 4-dioxane and urea. The nucleation rates were measured at low solute concentrations for alcohol and urea mixtures. A wider range is investigated for water + 1, 4-dioxane liquid mixture (up to 50 mol %).

The nucleation rate experiments that we carry out with single droplets in an electrodynamic trap, is used to examine the individual nucleation statistics. In this way we can accurately determine the nucleation rates at a given temperature near the homogenous nucleation limit. Our experiments are also distinguished as **temperature-jump** experiments, for which the droplets are not subjected to pre-cooling period. Instead, there occurs a temperature jump from the room temperature to the temperature of measurement.

5.2 Measurements of Nucleation Rates – The Electrodynamic Trap

The outline of the nucleation rate experiments can be given in the following key steps:

- a. Droplet generation.
- b. Levitation of single charged droplets
- c. Cooling of the trap and the temperature measurement.
- d. Determination of size and state of the droplets by elastic light scattering.
- e. Determination of homogeneous nucleation rates from the nucleation statistics.

Single droplets are generated using home-made, piezo-electric driven injectors. Droplets are charged by the use of an inert electrode, which is inserted into the sample vial. High voltage on the order of 2-3 kV is applied to the electrode. The injector is being fed from the sample vial through a Teflon capillary. The generated droplets have typical diameters in the range of 40-70 μm .

The electrodynamic trap consists of two copper ring electrodes placed in an octagonal shaped copper housing (see Fig. 5-1). Both AC and DC voltages are supplied to the rings. AC voltage is responsible for the time dependent electric field, thus forming the time dependent potential well through which a charged-droplet is trapped. DC voltage corrects the influence of the gravitational force. The trap is placed in a vacuum chamber which works as a thermal insulator.

The trap is cooled by circulating liquid nitrogen. The temperature is measured by a resistor thermometer Pt-100, which is placed near to the copper rings. The systematic error of the temperature calibration is found to be smaller than 0.25 K and the resolution of the temperature measurement to be 0.02 K (Stöckel 2001).

A He-Ne laser with $\lambda=632.8$ nm and $P=25$ mW was used for the detection of the state of the droplet and also for the estimation of its diameter.

5.2.1 Droplet Generation

Home-made⁴ piezo-injectors are used to generate the droplets. The construction of an injector is shown in Figure 5.2. The working principle is based on the contraction of a piezo-electric ceramic onto a glass capillary under fast-rising and short-lived rectangular voltage pulses. By this way pressure waves are created in the solution inside of the glass capillary, and the droplets are ejected from the open end. The open end of the glass capillary, where the droplets come out, is called the nozzle.

⁴ Erwin Biller: Department of Physical and Theoretical Chemistry, Freie Universität - Berlin.

The shape of a typical rectangular pulse exerted on the piezo-ceramic, and the time evaluation of a droplet with respect to the instance of applied pulse are also shown in Figure 4-2. The droplet attains a stable shape after a time delay of the applied pulse. It is also practiced that depending on the nature of the solution, and the individual characteristics of the capillaries, the strength and length of the applied rectangular pulse has to be varied to find the optimum condition.

The shapes of droplets that are ejected out of the nozzle are observed by “stroboscope effect” before they go into electrodynamic trap. An external CCD camera and a light emitting diode (LED), which is working at the same frequency of droplet generation, were used for this purpose: The CCD camera is focused at a point on the trajectory of a falling droplet, and the LED is positioned across the camera. When the light pulses emitted from the LED are in resonance with the droplet generation frequency, the image of the falling droplet can be caught by the CCD camera (see also Figure 5-3).

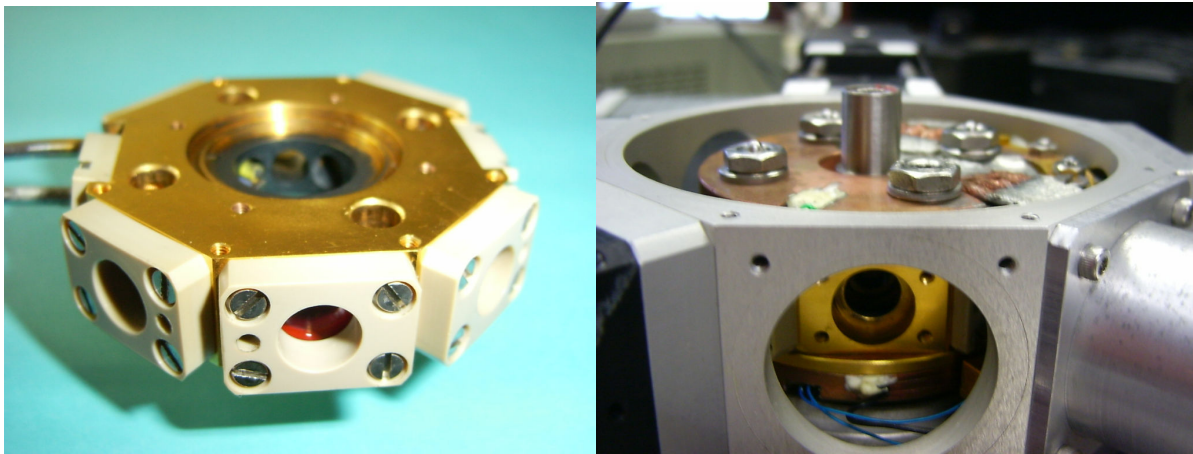
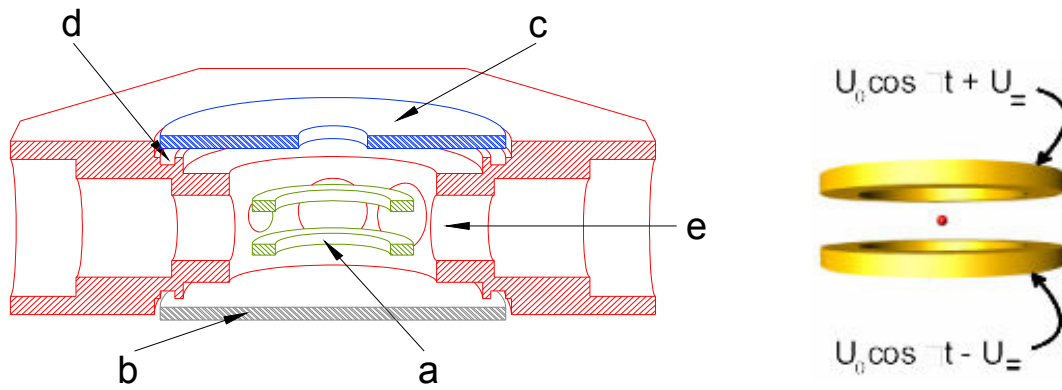
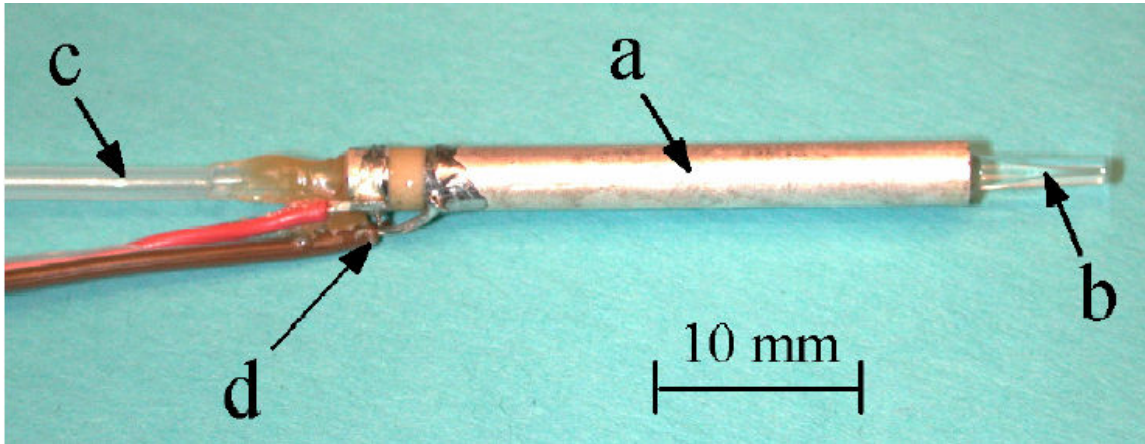
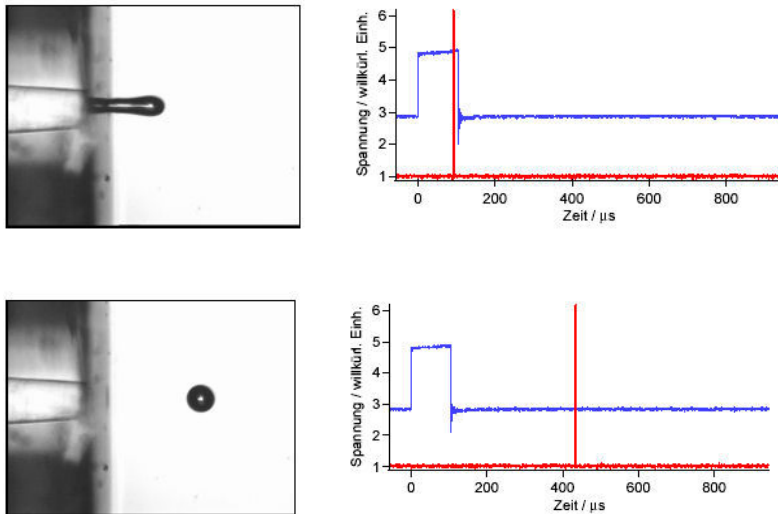


Figure 5.1: Upper left, the construction of the electrodynamic trap is drawn: a) ring electrodes b) bottom window c) opening for the falling droplet d) gas circulation e) optical port. Upper right the levitation of the droplet is illustrated. Below left the gold plated copper body of the trap is seen. Below right is the heating plate on top of the copper body, the falling tube and the vacuum chamber is seen in addition.



A-) The principle construction of a piezo-injector: a) piezoelectric ceramic that encases the glass capillary. b) Glass capillary - nozzle. c) Teflon-tube attached to glass-capillary for feeding solutions. d) Electrical connections to the inner and outer surface of the piezo-ceramic. Reproduced from (Stöckel 2001)



B-) A typical piezo-pulse and the state of the droplet relative to the phase of applied pulse Reproduced from (Stöckel 2001).

Figure 5.2: The construction of a piezo-injector and the droplet genesis.

While working with the aqueous solutions of solid substances (urea in this case) it is experienced that the solute precipitates on the surface of nozzle. This sometimes inhibits the generation of stable droplets. It may also result in the fluctuations of solute concentration in the micro droplets. Assuming the electronic peripheries that control the levitation of a droplet work stable inside the trap, the following factors should also be considered to successfully entrap a droplet:

- The droplets should be generated once at a time and should preserve their stability until they arrive into the trap.
- The nozzle should be positioned at the right place over the falling-tube that leads to the trap, so that the droplets should fall directly in to the center of the trap.
- The droplets should not deviate substantially from their paths, before they arrive in the center of the trap.

Charging of the droplets is achieved by putting an inert electrode into the sample vial, from which the injector is fed. High voltage on the order of 2-3kV is applied on this electrode. The charge carriers (which are being the OH^- and H_3O^+ in this case) with the opposite polarity of applied voltage is accumulated on the surface of the inert electrode. Accordingly the charge carriers with the same polarity of applied voltage are accumulated at the surface of the solution in the nozzle. By this way the droplets are charged with the same polarity of high voltage while they are being injected out. It was shown (Kramer and al 1999) that the electrical charge on the surface of the droplet, which is comparable to our case does not influence the nucleation event. During the experiments it was also shown that negative or positive polarity did not alter the results in the sensitivity of our measurements.

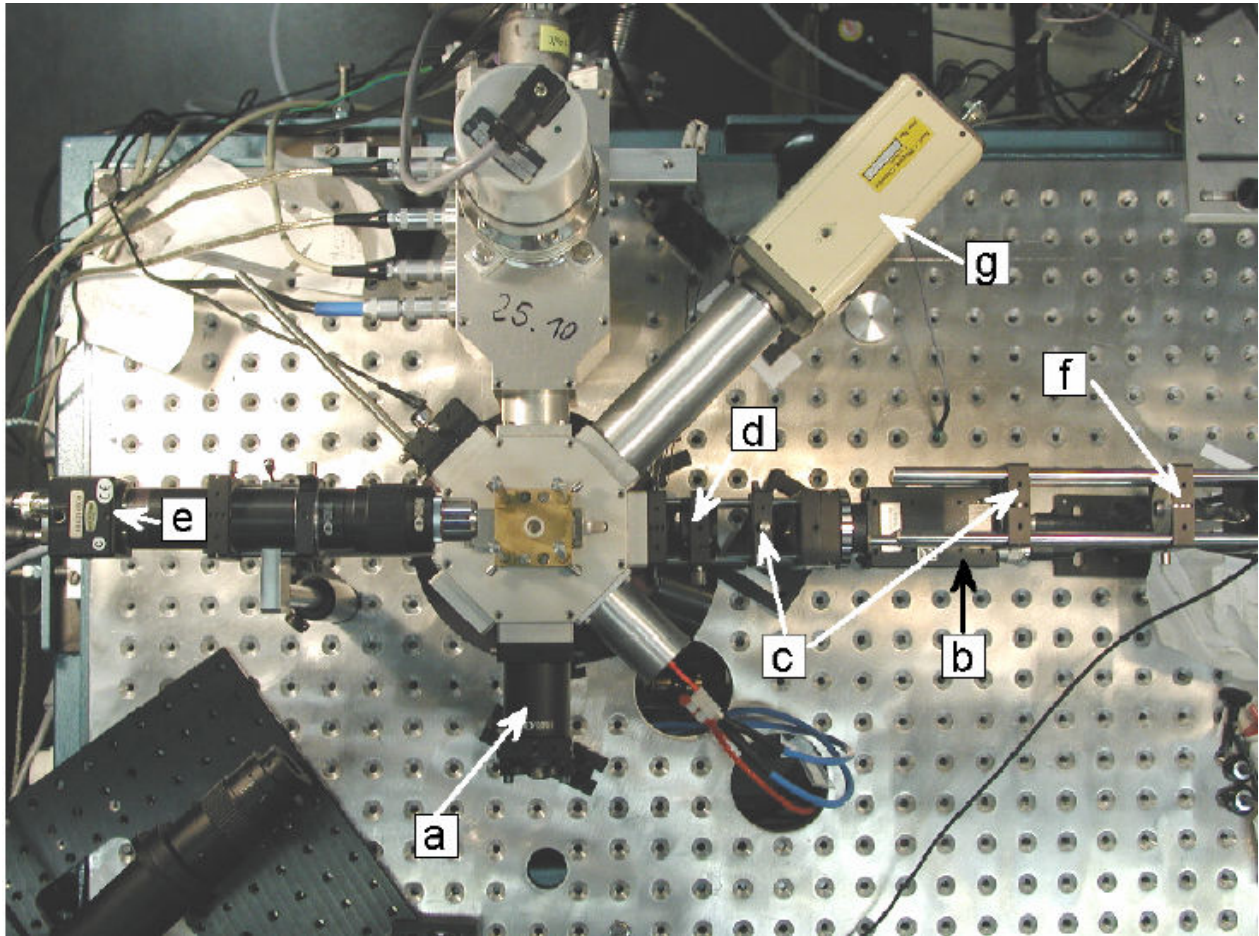


Figure 5.3: Top view of the experimental setup: a) Directing mirror for the laser light, b) CCD camera for the Mie analysis of scattered light, c) Focusing lenses, d) Polarization filter e) CCD camera used to observe the falling droplet, f) LED positioned across the CCD camera g) CCD camera for direct observation of the inside of the trap.

5.2.2 Levitation of the Droplets – The Electrodynamic Trap

It was first shown by Wolfgang Paul, that a charged particle can be levitated in a dynamically changing electric field.(Paul 1990) Such a field can be produced by the application of AC and DC voltages to certain electrode configurations. These systems are called as electrodynamic traps.

In our case, the trap consists of two copper ring electrodes that are placed in the center of a gold plated copper housing. The construction of the trap is schematically drawn in Figure 5-1. The ring electrodes are placed in such a way that one comes on top of the other with a certain distance. Both rings are connected to AC and DC voltage supplies.

Under the applied AC and DC voltages, an equation for the time dependent potential on the x, y, z directions at the center of the trap can be parameterized concerning the geometry of electrodes and their configurations:

$$V(t) = V_{DC} - V_{AC} \cos(\omega t) \quad (5-1)$$

$$V(x,y,z,t) = V_x(x,t) + V_y(y,t) + V_z(z,t) \quad (5-2)$$

In the next step these potentials can be used to solve the equation of motion for a charged particle:

$$m \times \frac{d^2 \vec{r}}{dt^2} = -q \nabla V \quad (5-3)$$

The outcome would be oscillatory Mathieu functions for the bound case. This means a charged particle will be confined to move in an orbit under the influence of a restoring force, which is a result of a pseudo potential created by a rapidly oscillating electrical field. The movement of the particle is limited to a very small region and does not effect the measurements.

The equation (4.4) indicates that a droplet's mass and charge will be involved in determining the stability conditions in the course of entrapment. As long as a droplet keeps its mass and charge constant, it will continue to be levitated. However, the droplets in the experiments are subjected to evaporation. It is observed during the experiments that the stability conditions for the droplets are lost after some time. This is mostly because the droplets lost their charges on the surface through evaporation and Coulomb explosions follow. In advance, droplet jets occur.

5.2.3 Cooling of the Trap

To cool down the trap, liquid nitrogen was circulated through a copper pipeline, which had a contact with the trap's body. The contact points were called as cooling fingers. After completing its cycle in the wire, nitrogen is given out. The flow of the nitrogen has a constant flux throughout the experiment.

For the thermal isolation, a vacuum is required in the space between the inner and outer body of the trap. By using a combination of two vacuum pumps, a vacuum of $10^{-4} - 10^{-5}$ mbar is achieved.

Two heating plates are placed up and down of the trap's body, to have a control on the temperature. The plates are heated up by passing current on them, when necessary. The amount of the current is controlled through a microcircuit. This way the temperature of the trap could be stabilized up to a precision of 0.02 °C.

5.2.4 Measurement of the Temperature

The temperature measurement inside the trap is done with Pt-100 resistance thermometer. The principle of the operation is to measure the resistance of the platinum element. The Pt-100 sensor has a resistance of 100 ohms at 0 °C. This resistance increases with increasing temperature and decreases with decreasing temperature.

According to the most recent definition of the relationship between resistance and temperature by International Temperature Standards 90 (ITS-90), the following equation is used:

$$R(T) = R_0 * (1 + A * T + B * T^2 + C * (T - 100) * T^3) \quad (5-4)$$

Where:

$$R_0 = 100 \text{ Ohms}$$

$$A = 3.9083 \text{ E-3}$$

$$B = -5.775 \text{ E-7}$$

$$C = -4.183 \text{ E-12 (below } 0 \text{ }^\circ\text{C), or}$$

$$C = 0 \text{ (above } 0 \text{ }^\circ\text{C)}$$

To obtain the temperature we need to measure the resistance of Pt-100 sensor. For this reason a small and constant sense current ($\sim 1\text{mA}$) is passed through the Pt-sensor, and the corresponding output voltage is measured. The measured voltage is transmitted to a personal computer via GPIB-Interface and converted to the equivalent resistance value. Subsequently a temperature value can be calculated by using a characteristic polynomial, which is similar to (5-4).

Due to series manufacturing process, it is not possible to exactly match the characteristics of every individual temperature sensor to the defined standards. A resistance-temperature sensor can deviate from the expected resistance behavior calculated from standardized $T(R)$ characteristics. For this reason, calibrations of the Pt resistance thermometers are done in the following way:

Two fixed points, $T_m(\text{Ice-H}_2\text{O})$ and $T_{\text{sub.}}(\text{CO}_2)$ are selected for the calibration of the temperature sensors. The characteristic polynomial given in (5-4) is re-adjusted to fit the measured value to the actual values at the fixed points. Linear error propagation is assumed in the measurement of temperature in between the fixed points.

How well the fit to the fixed points is, the temperature measurement can not be achieved with 100 % precision. This is mostly because two fixed points can not guarantee an exact match of the polynomial to the characteristics of the Pt-100 thermometer. Besides, the thermometers come

with tolerance limits. The thermometers that we use** belong to tolerance class B where the tolerance limit in measured temperature is defined by the following equation:

$$\Delta t = \pm (0.30 + 0.005 * |t|) \quad (5-5)$$

t: temperature, in °C.

The correctness of the calibrations was tested at varying times for both traps. Although it is observed that the calibrations continue to keep being valid, nucleation rate measurements with H₂O (tri-dist.) that were performed at different time periods in both traps, deviated from the previously determined values by Stöckel(Stöckel 2001). This is mostly due to the differences that occurred in the calibration of the temperature measurement in time.

5.2.5 Droplet Analyses by Elastic Light Scattering

The light scattering happens when non-uniformities occur in the medium through which an electromagnetic wave passes. If the scattering of light leads to some change in the energy of the radiation, it is called inelastic scattering. These types of scattering include Compton and Raman scatterings. On the other hand, no loss or gain of energy occurs in the elastic light scattering.

Three types of elastic light scattering are considered: For very big particles, where the wavelength of electromagnetic radiation is much smaller than the scattering particle, the rules of geometric optics apply. In the case of very small particles, where the wavelength (λ) of the scattered light is much bigger than the size of the particle, the Rayleigh scattering model is used. When the wavelength of the scattering light falls in a range, where it is on the order the size of scattering particles, Mie scattering theory is applied.

The size and state of the droplets are analyzed by elastic light scattering in the levitated microdroplet experiments. The scattered light source is a low-power (25mW) He-Ne Laser with the wavelength of 632.8 nm. The diameter of the droplets are varied in between $d = 40 - 70 \mu\text{m}$. This corresponded to a “size to wavelength” ratio of about 100, where Mie scattering theory is applicable.

** PCA style platin-chip-temperature sensors (Pt-100) – Class B, supplied from the manufacturer JUMO.

The mathematical treatment of light scattering in the framework of Mie scattering theory is given elsewhere (Stöckel 2001; Weidinger 2003). According to Mie theory of light scattering, the intensity of a scattered light will depend strongly on the angle of observation. To calculate the intensity of a scattered light at a particular angle of observation, one needs to know the intensity, wavelength and the polarization of the incident light, as well the refractive index and the size of the scattering particle. Once these parameters are identified, the theoretical intensity profiles can be calculated as a function of angle. Figure 5.4 shows in this manner the calculated Mie scattering intensity of a perpendicular polarized light for various sizes of droplets with the scattering angle of 80 to 100 degrees.

During the experiments the scattered light intensities of a polarized He-Ne laser light ($\lambda = 632.8$ nm) from the droplets is collected within an angular range of about 20° centered at 90° . The optical setup necessary to carry out this task is illustrated in Figure 5.5. A CCD camera is placed at a position vertical to the direction of incident laser light that corresponds to a 90° scattering angle. The light scattered on the direction of the camera from a droplet at the center of the trap is collected and parallelized through an achromatic biconvex lens (L1), and focused on the light sensitive area of the CCD chip through a second biconvex lens (L2). A polarization filter is placed in between the two lenses (L1) and (L2), which acts as an analyzer for the state of the droplets.

This filter is consisted of two parts: The upper-half allows only the perpendicular polarized light to pass along, and the lower-half allows parallel polarized light to pass. Consequently two channels are reserved in the data acquisition software corresponding to two polarizations.

Just after a droplet is levitated at the center of the trap, a sudden rise of intensity will be detected in the perpendicular-polarized channel of the image acquisition system. This time instance will be noted as t_0 by the data acquisition software. As long as the droplet stays liquid, the polarization of the scattering light will be conserved, and the radiation will be allowed to pass only along the upper side of the filter. As soon as the droplet is frozen, the light will be depolarized upon scattering, i.e. the scattered waves will be composed of all kind of polarizations. This event leads to the detection of light intensity also in the parallel-polarized channel. It is taken as the

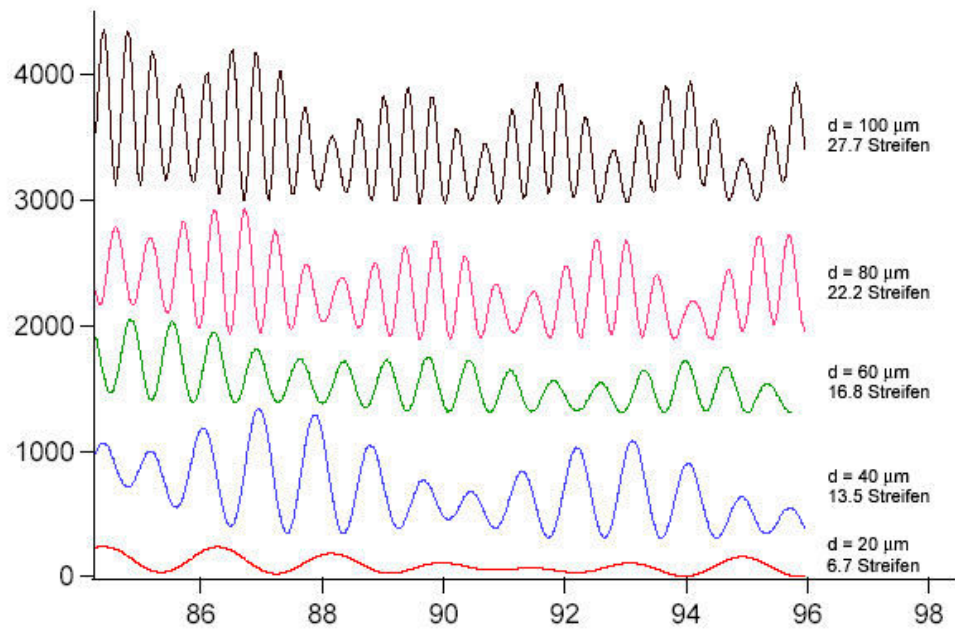


Figure 5.4: Mie-scattering intensity of perpendicularly polarized light calculated for various sizes of droplets in the angular region of experimental interest.

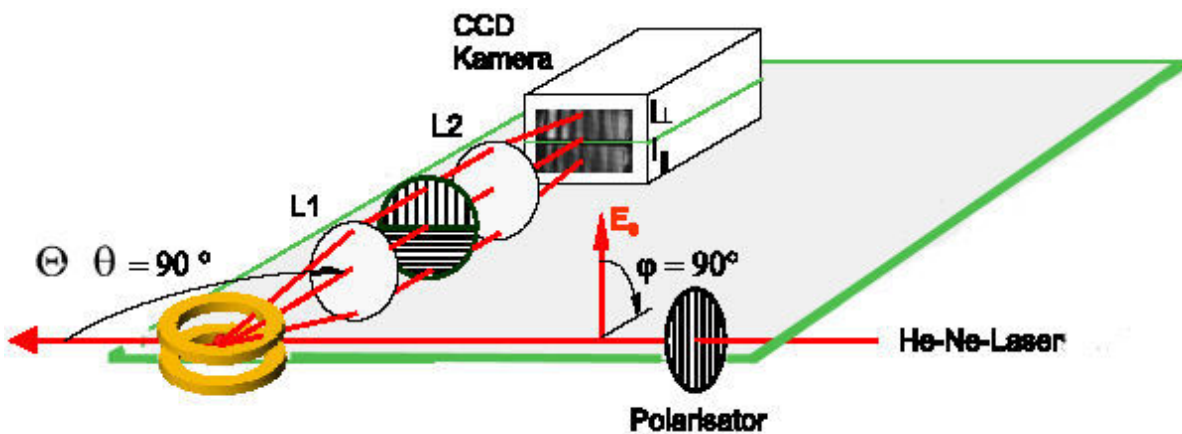


Figure 5.5: The optical setup of the experiment.

indication of a phase transition in our experiments, and noted as t_n . Accordingly $t_n - t_0$ gives the nucleation time.

5.2.6 Calibration of the Image Acquisition System

The image acquisition system requires calibration for the precise measurement of droplet sizes. This is because the Mie light scattering intensity depends strongly on the scattering angle.

In the experiments the scattered light is collected on a CCD camera from an angular region centered at 90° . The width of the angular region is limited by the aperture of the trap's body, where a collecting lense is placed. This aperture has a radius of $r = 4.4$ mm, and its distance to the center of the trap is $d = 14$ mm. Therefore the width of the angular region is determined as

$$\theta = 2 * \arctan(r/d) = 17.86^\circ \quad (5-6)$$

This value can be further limited by a computer program. This is done by defining “region of interests” that is used to crop the obtained camera image. In this manner, the angular width of the region of interests (ROI) was chosen to be 11.7° ($84.3 < \theta < 96.0$), which is smaller than the physically accessible limits.

The theoretically calculated intensity profiles of the scattering light from water droplets of various sizes are given earlier in Figure 5.4. It is seen in the figure that the number of peaks in the intensity profiles are closely related to the size of the droplets. When the droplet is at liquid state, the polarization of the incident light is conserved after the scattering event. Consequently the scattered waves can interfere constructively and destructively to give regular scattering patterns. The camera images of these patterns will be consisted of stripes, alternating in bright and dark regions (see also Figure 5.6). Therefore the number of bright stripes in the camera images is proportional to the number of peaks (intensity maxima) in the intensity profiles, which in turn is related to the size of the droplets.

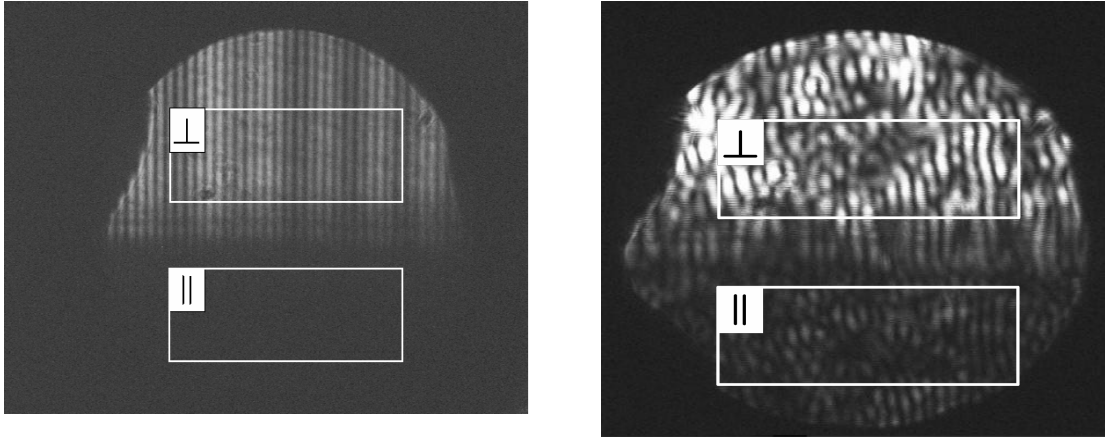


Figure 5.6: The camera images of a droplet taken at a 90° scattering angle before (on the left) and after (on the right) freezing.

A linear relation is obtained in between the droplet diameter and the number of stripes by calibrating the image acquisition system. Thus the determination of droplet size in the experiments is achieved by counting the stripes belonging to the captured image of the scattering pattern of a droplet by the help of a computer program. This was then converted to the corresponding length of the droplet's diameter according to the linear relation obtained in the calibrations.

5.2.7 Determination of Homogenous Nucleation Rates

The process of homogeneous nucleation can be described by Poisson statistics. The probability for the formation of a nucleus at a certain time in a certain volume element of the droplet is assumed to be independent of the position of the volume element inside the droplet and the time of freezing. Integration of the statistical law in the limits of many observed events gives (Kramer, Hübner et al. 1999):

$$\ln (N_u(t)/N_0) = -J(T) \cdot V_d \cdot t \quad (5-7)$$

Here $N_u(t)$ is the number of unfrozen droplets after time t , N_0 is the total number of investigated droplets. V_d is the volume of the droplet and $J(T)$ is the temperature dependent nucleation rate.

A derivation of the nucleation rate equation (5-7) is given in detail by Pruppacher and Klett (Pruppacher and Klett 1997). These authors considered a population of N_0 isolated water drops, all having the same temperature T and the same volume V_d . They further assumed that a nucleation event in any one drop is independent of that in any other one. If a temperature dependent nucleation rate $\mathbf{J(T)}$ is defined at these conditions, the number of ice germs produced during the time dt in the volume $N_u V_d$ of unfrozen water is given as:

$$N_g(t + dt) - N_g(t) = NuV_d \cdot J(T)dt \quad (5-8)$$

Just after a nucleation event in a drop occurs, the drop will rapidly grow to an ice particle. This is because the growth velocity of ice is very large in comparison to formation of a critical nucleus, at the supercoolings where homogeneous ice nucleation takes place. Therefore, the authors supposed that the ice formation is the result of only one nucleation event per drop. At these conditions the increase in the number of frozen drops dN_f will be equal to the number of ice germs produced in time dt :

$$dN_f = NuV_d \cdot J(T)dt \quad (5-9)$$

Since the total number of N_0 droplets is constant we have $dN_u = -dN_f$. The equation (5-9) becomes:

$$dN_u = -NuV_d \cdot J(T)dt \quad (5-10)$$

Integrating (5-10) from N_0 at $t = 0$ to N_u at t , we arrive at the expression, which describes the decrease in the number of unfrozen drops with increasing time at a constant temperature:

$$N_u = N_0 \exp[-V_d \cdot J(T)t] \quad (5-11)$$

Eq. (5-11) is in fact a first order rate equation (with an extra volume normalization factor). As well, it is used to describe the decay of radioactive isotopes. In this manner, (5-11) is used to

describe the activity of a radioactive substance containing many radioactive isotopes of the same kind, where the decay constant (λ) substitutes for $V_d \cdot J(T)$. Indeed, the decay of an isotope into a different isotope and the growth of a droplet into an ice particle have the same statistical origin. The freezing events, like radioactive decays, is described by Poisson statistics:

The probability that out of a N_0 drops, N_f drops have frozen during the time interval $t = 0$ to $t = t_f$ is:

$$P(N_f, t_f) = \frac{(\lambda t_f)^{N_f} \exp(-\lambda t_f)}{N_f!}, \quad N_f = 0, 1, 2, \dots \quad (5-12)$$

with $\lambda = V_d J(T)$. The probability that during the time interval $t = 0$ to $t = t_f$ no freezing events take place is then

$$P(N_f = 0, t_f) = \exp[-V_d J(T)t_f] \quad (5-13)$$

Identifying $P(N_f = 0, t_f)$ with (N_u/N_0) , i.e. with the ratio of the N_u drops survived freezing to the whole population of drops, equation (4-11) is recovered. (Pruppacher and Klett 1997)

During the experiments we obtain the nucleation time t_n of each drop at a constant temperature T . To get the nucleation rate from this information we rearrange equation (5-11) as:

$$\ln(N_u/N_0) = -J(T) \cdot V_d \cdot t \quad (5-14)$$

If we plot the natural logarithm of the survival probability of unfrozen droplets versus $V_d \cdot t$, we obtain the negative value of the nucleation rate $J(T)$ from the slope according to equation (4-14). An exemplary case is given in Figure 4.7 for $\ln(N_u/N_0)$ vs $V_d t$ diagrams. The diagram in Figure 4.7 is obtained from the nucleation rate measurement of tri-distilled water at 36.03 °C. More than three hundred droplets are analyzed in terms of their volumes and nucleation times for this purpose. In the diagram, the x-axis denotes the nucleation time of droplets multiplied by their volumes. Consequently each point on the diagram corresponds to the volume-normalized probability of unfrozen droplets at a time t , for the y axis. The nucleation rate is obtained from the absolute value of slope of the best-fit line. Yet

again in analogy to radioactive decay similar diagrams are used to plot the activity of a radioactive substance. This time the slope corresponds to the decay constant.

As discussed in the evaluation of experimental results, substantial deviations from the linearity occurs for some of the $\ln(N_u/N_0)$ vs $V_d t$ diagrams. In the simplest case they are treated as anomalies. However, many factors could take part in occurrence of non-linear behavior. For particular cases it might be occurring as a result of the nature of an aqueous solution.

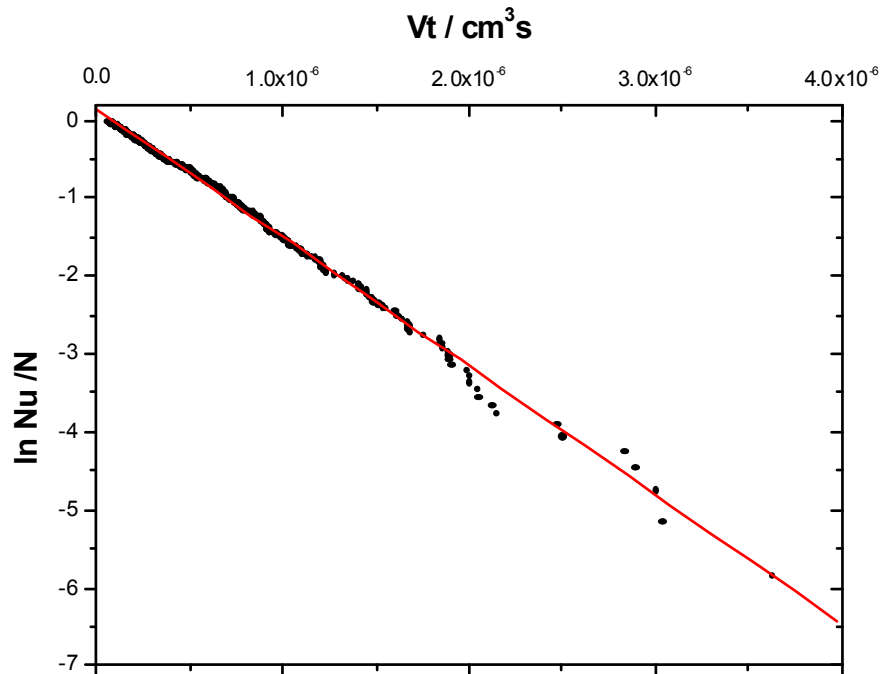


Figure 5.7: $\ln N_u/N_0$ vs $V_d t$ diagram obtained from the nucleation rate measurement of tri-distilled water at 36.03 °C. A total of 341 single droplets are analyzed in terms of their volumes and nucleation times. The red line is the best fit to the linear progression of data points. According to equation (4-14) the negative of the slope of this best-fit line gives us the temperature dependent nucleation rate $J(T)$. It is obtained from the above diagram as $J(36.03)_{H_2O} = 1.65 \text{ E}6$.

5.3 Substances and Preparation of Solutions

5.3.1 Substances

The chemicals are obtained from Aldrich and Merck. Their qualifications are given as below:

Ethanol – $C_2H_5(OH)$: Absolute, 99.9 %, Sigma-Aldrich, Germany.

2-propanol (isopropanol) – $C_3H_7(OH)$: Water-free, 99.5 %, Aldrich, Germany.

1,2-ethanediol (glycol) – $C_2H_4(OH)_2$: Water-free, 99.8 %, Aldrich, Germany.

1,4-dioxane – $C_4H_8O_2$: Water-free, 99.8%, Aldrich, Germany.

Urea – CH_4N_2O : 99.5%, Merck, Germany.

5.3.2 Preparation

The solutions with the mole fractions of solutes given in table 4.1 are prepared by weighing necessary amount of solute and tri-distilled water into a volumetric flask, and stirring them for thirty minutes by an automated shaker. The solutions are usually prepared freshly on the day of the experiment, otherwise kept closed in their flasks, and consumed in two weeks.

Before the experiments, small amount of a given solution is transferred into a 4 ml sample vial. The solutions are filtered through disposable syringe filters of pore size 0.2 μm while they are being filled into the vials. The vial is closed on top with screw caps and silicon/Teflon-coated septa.

Experiments are repeated several times at each particular composition, with newer solutions to ensure the reproducibility of obtained results and observations. The solution in the vial is consumed after 2-3 days; new vials are used if it is necessary to measure further.